Nanotechnology

PAPER

Superior sponge-like carbon self-doping graphitic carbon nitride nanosheets derived from supramolecular pre-assembly of a melamine–cyanuric acid complex for photocatalytic H_2 evolution

To cite this article: Lingfeng Li *et al* 2021 *Nanotechnology* **32** 155604

IOP Publishing Nanotechnology
Nanotechnology 32 (2021) 155604 (10pp) https://doi.org/10.1088/1361-6528/abd6d1

Superior sponge-like carbon self-doping graphitic carbon nitride nanosheets derived from supramolecular pre-assembly of a melamine–cyanuric acid complex for photocatalytic H_2 evolution

Lingfeng Li, Juhua Zhang, Quan Zhang, Xiaohao Wang and Wei-Lin Dai

Department of Chemistry and Shanghai Key Laboratory of Molecular Catalysis and Innovative Materials, Fudan University, Shanghai 200433, People's Republic of China

E-mail: wldai@fudan.edu.cn

Received 26 October 2020, revised 3 December 2020
Accepted for publication 25 December 2020
Published 25 January 2021

Abstract

The photocatalytic evolution of hydrogen (H_2) from water splitting is considered a promising route to overcome the energy crisis, and the key lies in the preparation of efficient photocatalysts. Herein, superior ordered sponge-like carbon self-doped graphitic carbon nitride (g-C_3N_4) nanosheets (SCCNS) were prepared via a combined strategy of melamine–cyanuric acid complex supramolecular pre-assembly and solvothermal pre-treatment using ethylene glycol (EG) aqueous solutions (EG:water = 50:50 vol.%) as a solvent and carbon doping source. The following pyrolysis converts the naturally arranged melamine–EG–cyanuric acid supramolecular intermediates to highly crystalline SCCNS with large specific surface areas. The optimal SCCNS-180 exhibits superior photocatalytic H_2 evolution activities (~4393 and 11 320 μmol h^{-1} g^{-1}) when irradiated with visible light and simulated sunlight; these values are up to ~17- and ~18-fold higher than that of bulk g-C_3N_4. The quantum efficiency of SCCNS-180 at λ = 420 nm can reach 6.0%. The excellent photocatalytic performance of SCCNS-180 derives from its distinct ordered sponge-like nanosheet structure with highly crystallinity and the carbon doping, leading to its improved optical absorption, accelerated photoinduced electron–hole pair transfer and separation rate and enlarged specific surface area (134.4 m^2 g^{-1}).

Supplementary material for this article is available online

Keywords: carbon self-doped, graphitic carbon nitride nanosheets, supramolecular pre-assembly, highly crystalline, photocatalytic H_2 evolution

(Some figures may appear in colour only in the online journal)

1. Introduction

Due to the over-consumption of fossil fuels in recent years, the energy crisis is being aggravated day by day. Thus, alternative green and renewable energy sources need to be developed to tackle the energy shortage problem [1–4]. The photocatalytic splitting of water for hydrogen (H_2) evolution using solar energy is viewed as a promising route because of the inexhaustible solar energy source and the abundant water resources on Earth [5–9]. Thus, various semiconductor photocatalysts have been developed for UV- or visible-light-driven H_2 evolution, including TiO_2 [10], $BiVO_4$ [11], Bi_2WO_6 [12], Ag_3PO_4 [13], CdS [14] and Fe_2O_3 [15]. However, the wide band gap metal oxide semiconductors, such as Ta_2O_5 (~4.0 eV), ZnO (~3.4 eV) and TiO_2 (~3.2 eV), exhibit a low utilization rate of solar energy because of their

limited sunlight absorption range. Thus, several photocatalysts with a narrow band gap and a suitable band structure, including metal nitrides, metal phosphides and metal sulfides, have also been studied for photocatalytic H_2 evolution, for example InN (∼1.1 eV), Ni_2P (∼1.0 eV) and CdS (∼2.4 eV). However, the disadvantages of auto-oxidation and photocorrosion dramatically limit their further applications [16]. Recently, graphitic carbon nitride (g-C_3N_4) has attracted tremendous interest since Wang and his colleagues reported in 2009 that, when irradiated with visible light, g-C_3N_4 could drive water splitting to produce H_2 and O_2 [17]. As a promising nonmetallic semiconductor photocatalyst, g-C_3N_4 can utilize visible light ($\lambda < 460$ nm) effectively to split water for H_2 evolution, owing to its appropriate band gap (∼2.7 eV) and suitable energy level position. It also exhibits excellent chemical stability (against organic solvents, alkali and acid) as well as thermal stability (stable at <600 °C in air) [18]. In addition, g-C_3N_4 can easily be obtained by direct thermal polycondensation of N-rich precursors, including urea [19], thiourea [20], cyanamide [21, 22], melamine [23], ammonium thiocyanate [24] and dicyandiamide [25]. Moreover, chemical exfoliation can functionalize it easily [26]. g-C_3N_4 is acknowledged as a promising photocatalyst with great potential for photocatalytic H_2 production because of its tremendous advantages, such as ease of preparation, a proper energy band structure, easy functionalization, abundance and outstanding physicochemical stability [27–29]. However, the traditional method for preparing bulk g-C_3N_4 (bulk-CN) via direct thermal polymerization of N-rich precursors generally has many shortcomings, including a disordered structure, limited specific surface area, high photoinduced electron–hole pair recombination rate, limited electroconductibility and limited visible-light utilization (<460 nm) [30, 31]. Thus, for its specific applications it is crucial to produce g-C_3N_4-based photocatalysts with an ordered structure, increased specific surface area, enhanced photoabsorption, improved electrical conductivity and lower charge carrier recombination rate – and thus enhanced photocatalytic performance. Great efforts have been made to prepare g-C_3N_4 with high catalytic performance, for example to composite it with non-noble metal cocatalysts [32–38], noble metals, conductive materials or semiconductors [39]. It is also feasible to promote the photocatalytic properties of g-C_3N_4 by synthesizing thinner, well-organized, porous, highly crystalline and doped g-C_3N_4-based materials [40–42], and a supramolecular pre-assembly strategy has been proved as a promising route to prepare ordered and morphologically controllable g-C_3N_4. However, the supramolecular pre-assembly strategy can produce a relatively low crystallinity because of the incomplete polycondensation reaction. Interestingly, in recent years, melamine precursor hydrothermal pre-treatment has been proved as a feasible and efficient method to prepare highly crystalline g-C_3N_4 with a large specific surface area [43, 44]. Furthermore, non-metal doping was found to be a feasible route to optimize the electronic structure and photocatalytic performance of g-C_3N_4. However, anion doping has several drawbacks, including a reduction in the reducibility of photogenerated electrons. Moreover, the external impurities may act as recombination centers for photoinduced charge carriers. Dong's group have reported that the energy band and intrinsic electronic structure of g-C_3N_4 can be changed via carbon self-doping, thus extending its visible light absorption range and promoting its electroconductibility and photoreduction performance, while no impurities and defects were incorporated [45].

Herein, an alternative facile method was developed to produce sponge-like carbon self-doping g-C_3N_4 nanosheets (SCCNS) via direct calcination of the solvothermally pre-treated cyanuric acid–melamine supramolecular complex in ethylene glycol (EG) aqueous solution, in which EG can act as a solvent as well as the carbon doping source to build cyanuric acid–EG–melamine complexes. Consequently, the solvothermal temperature greatly affects the physicochemical properties of the as-prepared photocatalysts. That is, the desired superior carbon self-doping g-C_3N_4 nanosheets can only be obtained at an appropriate solvothermal temperature. The optimal SCCNS sample was successfully obtained at a solvothermal temperature of 180 °C (SCCNS-180). In particular, the as-obtained optimal SCCNS-180 exhibited enhanced optical absorption, accelerated photoinduced electron–hole pair separation and transfer rate, a superior electronic band structure and a larger specific surface area. Thus, the as-obtained SCCNS-180 displays dramatically improved photocatalytic activities for H_2 evolution (∼4393 and 11 320 μmol h^{-1} g^{-1}), values which are ∼17- and ∼18-fold those of the bulk-CN (∼258 and 620 μmol h^{-1} g^{-1}) when irradiated with visible light ($\lambda > 400$ nm) and solar irradiation, respectively. Besides, the quantum efficiency (QE) of SCCNS-180 at a wavelength of 420 nm reaches 6.0%, indicating its relatively good visible light utilization.

2. Experimental methods

2.1. Synthesis of photocatalysts

To synthesize BCN 6 g of melamine was placed in a crucible which was wrapped with Al foil. Afterwards, the crucible was heated at 550 °C for 3 h under a nitrogen atmosphere in a quartz tube furnace, at a heating rate of 5 °C min^{-1}.

For the SCCNS-T (T means the treated temperature) samples, first 0.5 g of cyanuric acid and 0.24 g of melamine were respectively dissolved into 55 and 15 ml of hot EG aqueous solution (90 °C) (EG:water = 50:50 vol.%) under continuous stirring. The molar ratio of cyanuric acid to melamine was set at 2:1. After complete dissolution, the melamine solution was slowly dropped into the cyanuric acid solution and a white precipitate was quickly produced, which was kept stirred for 30 min. Then, the as-obtained white suspensions were transferred to a 100 ml Teflon-lined autoclave and heated at 160, 180 and 200 °C for 24 h, respectively (as shown in scheme 1). After cooling down to room temperature, the white precursors were centrifuged, washed thoroughly with distilled water and ethanol three times respectively, then dried at 100 °C in an electric oven over night. SCCNS-T samples were finally prepared by heating the white solid at 550 °C for 3 h in a tube furnace at a heating rate

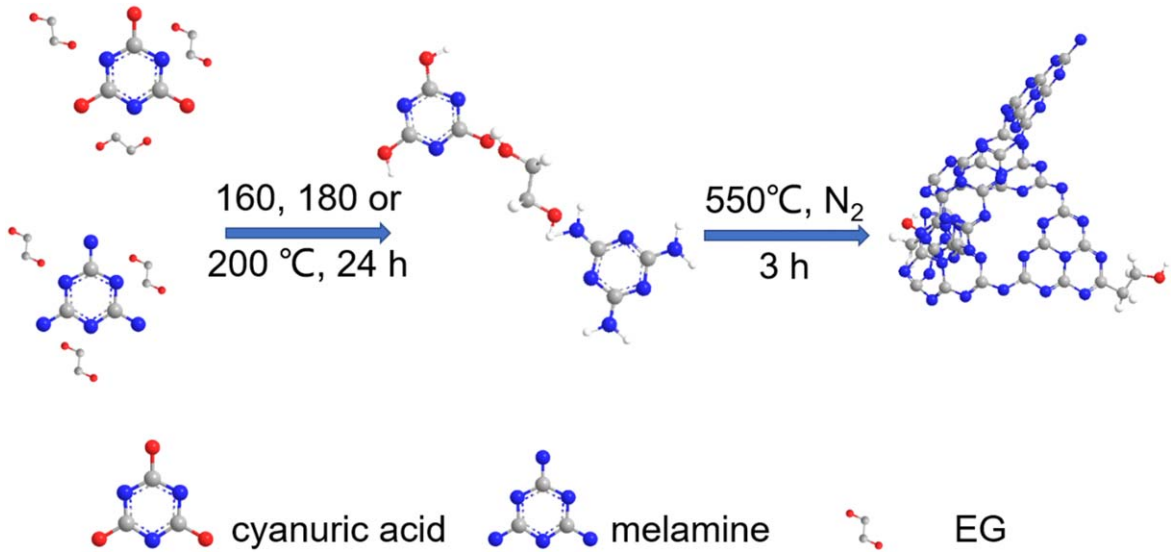

Scheme 1. The process for preparation of SCCNS-T samples.

of 5 °C min^{-1} under a N_2 atmosphere. Finally, the as-obtained products were collected as SCCNS-160, SCCNS-180 and SCCNS-200, respectively. Other solvothermal parameters that may affect the photocatalytic activities of SCCNS-T, including the molar ratio of cyanuric acid to melamine (0.5–3.0), the solvothermal time (18–30 h) and the annealing temperature (500–570 °C), were also optimized to maximize the photocatalytic H_2 evolution performance. Moreover, the supramolecular pre-assembly precursor was calcined directly without solvothermal pre-treatment and labeled as pristine-CN (figure S1, available online at stacks.iop.org/NANO/32/155604/mmedia) for comparison.

2.2. Characterization, photoelectrochemical and photocatalytic activity tests

Detailed descriptions of the characterization methods and photoelectrochemical and photocatalytic activity tests can be found in the supporting information.

3. Results and discussion

The crystal structure of the bulk-CN and various SCCNS-T samples was investigated by x-ray diffraction (XRD). As shown in figure 1(A), all samples exhibited typical diffraction peaks characteristic of g-C_3N_4, i.e. a remarkable peak at ~27.7° and a weak peak at ~13.0°, consistent with previous reports [46]. For bulk-CN, the peak corresponding to the interlayer aromatic segment stacking is located at 27.7°, and is ascribed to a typical (002) lattice plane, while the peak corresponding to the in-plane tri-*s*-triazine units is located at 13.0°, and is ascribed to the (100) phase [47, 48]. The (002) diffraction peak of SCCNS-180 shifted to a higher angle (28.2°) compared with bulk-CN (27.7°), indicating that the interlayer stacking distance of SCCNS-180 was reduced from that of bulk-CN, which can be more conducive to charge carrier separation and transfer between the interlayers of SCCNS-180. The reduced interlayer stacking distance of SCCNS-180 can be ascribed to a combination of melamine–cyanuric acid supramolecular complex pre-assembly and solvothermal pre-treatment at moderate temperature, giving the as-prepared SCCNS-180 an ordered and highly crystalline structure. This result implies that the SCCNS-180 exhibited a much enhanced charge carrier separation rate and thus a much improved photocatalytic activity for H_2 production [49]. Moreover, FTIR spectroscopy was used to obtain physico-chemical structural information about the samples (figure 1(B)). It was found that the IR bands of all SCCNS-T samples are consistent with those of bulk-CN, suggesting that the chemical structure of all SCCNS-T samples is nearly identical to bulk-CN. As we know, the peaks around 808 cm^{-1} belong to the characteristic *s*-triazine unit out-of-plane skeletal bending modes, and the enhanced peaks in SCCNS-180 indicate the reduced molecular layers in SCCNS-180, which can be favorable for photoinduced charge carrier separation and transmission [50–52]. In addition, the weak peak near 808 cm^{-1} may be ascribed to the doping carbon which might replace some of the nitrogen sites. The peaks at about 1200–1800 cm^{-1} belong to the sp^2 C=N stretching vibration modes [53]. Meanwhile, the broad band between 3000 and 3600 cm^{-1} is assigned to the $-NH_2$ groups or the surface-absorbed H_2O molecules. Enhanced absorption between 3000 and 3600 cm^{-1} of the SCCNS-180 sample is clearly seen, suggesting that SCCNS-180 has a larger exposed surface than the other samples [49, 54, 55].

To investigate the specific surface area and the porous structure of the samples, N_2 absorption–desorption isotherms of all samples were obtained (figure 1(C)). All samples displayed a similar type IV isotherm shape. Moreover, compared with bulk-CN, all SCCNS-T samples exhibited a much enlarged specific surface area (see table S1 for details). The Brunauer-Emmett-Teller (BET) surface areas of SCCNS-160, SCCNS-180 and SCCNS-200 are measured to be 47.2, 134.4 and 45.3 $m^2 g^{-1}$, which are all much larger than that for bulk-CN (16.5 $m^2 g^{-1}$).

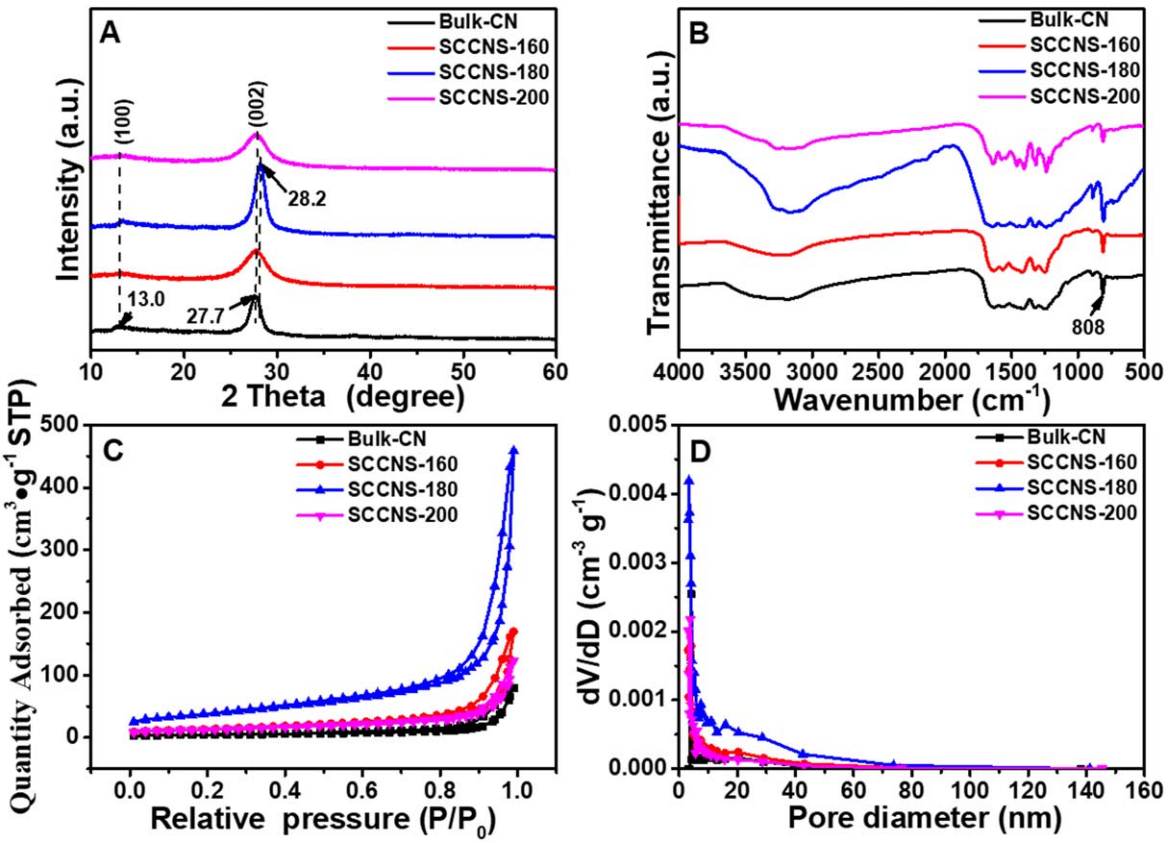

Figure 1. XRD patterns (A), FTIR spectra (B), N_2 adsorption/desorption isotherms (C) and pore size distribution (D) of bulk-CN and various SCCNS-Ts.

In particular, SCCNS-180 has a BET area more than eight-fold higher than bulk-CN. The pore size distribution can be seen in figure 1(D). Both bulk-CN and SCCNS-T exhibit a similar pore size distribution range (~3–140 nm); however, SCCNS-180 shows a broader distribution range (6–40 nm), suggesting a well-generated mesoporous structure. The average pore diameter and total pore volume of all samples are shown in table S2. Although bulk-CN exhibits a slightly larger average pore diameter (~30 nm) than SCCNS-T samples (~17–22 nm), the total pore volume of all SCCNS-T samples (0.19–0.71 $cm^3\ g^{-1}$) is still larger than that for bulk-CN (0.12 $cm^3\ g^{-1}$), especially SCCNS-180 (0.71 $cm^3\ g^{-1}$), which has about a six-fold greater pore volume than bulk-CN. The increased surface area and pore volume of SCCNS-180 derive from its unique sponge-like nanosheet structure. Significantly, the greatly increased surface area and pore volume of SCCNS-180 give it more reactive sites as well as the conversion rate of H_2O to the desired H_2, resulting in its dramatically enhanced photocatalytic activity [56].

To further determine the micromorphology and structure of different SCCNS-T samples they were examined by scanning electron microscopy (SEM) and transmission electron microscopy (TEM) (figures 2(A)–(C) and (D)–(F)). It was found that the solvothermal pre-treatment temperature in this work affected the morphology and structure of SCCNS-T samples dramatically. That is, when the solvothermal pre-treatment temperature was just 160 °C, the as-obtained SCCNS-160 sample exhibited a disordered and irregular shape (shown in figures 2(A) and (D)). When the solvothermal temperature was increased to 180 °C, the as-prepared SCCNS-180 sample became much ordered, with a regular sponge-like nanosheet structure with some wrinkles (figures 2(B) and (E)). Moreover, the SCCNS-180 nanosheets exhibited remarkable curvature at the edge of the sheets. As shown in figure S 2(A), the dark contrast lines at the end of the sheet are believed to be the standing edges or wrinkles of the nanosheets. Such distortion of the two-dimensional nanosheet structure can be stabilized, a situation which is also found in single-layered graphene [57]. High-resolution TEM (HRTEM) images were also obtained for SCCNS-180 to identify the surface structures (figure S 2(B)); SCCNS-180 exhibited a thin nanosheet structure with some wrinkles. Moreover, lattice fringes of about 0.67 and 0.33 nm were observed, attributed to typical g-C_3N_4 (100) and g-C_3N_4 (002) and consistent with the XRD results, indicating that the as-obtained SCCNS-180 still possesses a typical g-C_3N_4 structure after carbon self-doping. The unique ordered sponge-like nanosheet structure of the SCCNS-180 sample could give it enhanced optical absorption, improved charge carrier separation and transfer rate and an enlarged surface area and thus more exposed reactive sites. Consequently, SCCNS-180 could show a much improved photocatalytic H_2 evolution. However, with further increase in the solvothermal pre-treatment temperature to 200 °C, the as-obtained SCCNS-200 sample becomes disordered again as shown in figures 2(C) and (F), which will not favor its photocatalytic activity. The field emission TEM (FETEM) and corresponding elemental distribution results for SCCNS-180 are

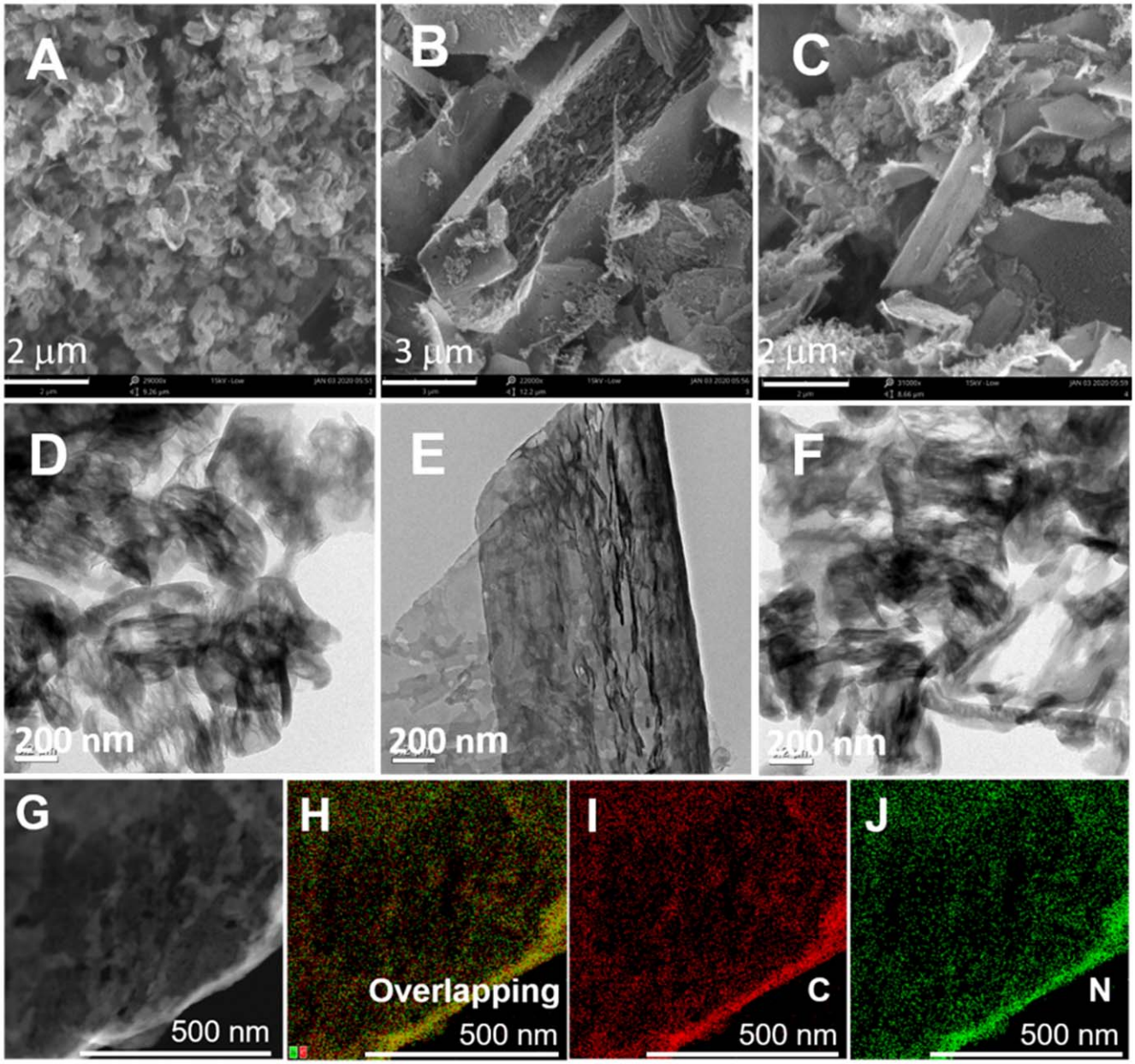

Figure 2. Micromorphology and structure of different SCCNS-T samples: SEM (A)–(C) and TEM (D)–(F) of SCCNS-160, SCCNS-180 and SCCNS-200, respectively; FETEM (G) and the corresponding elemental mappings of SCCNS-180 for overlapping of C and N (H), C (I) and N (J) elements.

shown in figures 2(G)–(J), demonstrating that C and N are uniformly distributed in SCCNS-180. STEM-EDX was also carried out for bulk-CN, SCCNS-160, SCCNS-180 and SCCNS-200 to investigate their elemental composition (see table S3). It was found that the carbon atomic concentrations of SCCNS-160 (51.33%), SCCNS-180 (56.15%) and SCCNS-200 (55.77%) were all higher than that of bulk-CN (49.86%), indicating the successful carbon doping in SCCNS-T samples.

The surface compositions of bulk-CN and SCCNS-180 were further investigated by x-ray photoelectron spectroscopy (XPS), as shown in figure 3. Both bulk-CN and various SCCNS-180 samples exhibit two sharp peaks at ∼284 and ∼398 eV (figure 3(A)), ascribed to C 1s and N 1s, respectively. Moreover, two peaks corresponding to C–C/C=C and N=C–N can be seen in the high-resolution XPS spectra of C 1s for both bulk-CN and SCCNS-180, with the binding energies located at ∼284.6 and ∼288.2 eV (figure 3(B)). Furthermore, the area ratios of the peaks at 284.6 and ∼288.2 eV were calculated as 0.054 and 0.061 for bulk-CN and SCCNS-180, respectively. The relatively increased C–C/C=C component of SCCNS-180 certified the successful carbon doping in SCCNS-180. Figure 3(C) shows the N 1s spectra of bulk-CN and SCCNS-180, among which four peaks can be observed at binding energies of ∼398.6, ∼399.7, ∼400.9 and ∼404.3 eV, which are ascribed to the C–N=C, N–$(C)_3$ and N–H groups and the π-electron delocalization in g-C_3N_4 heterocycles, respectively. Moreover, the area ratios of the peaks at 399.7 eV for SCCNS-180 compared

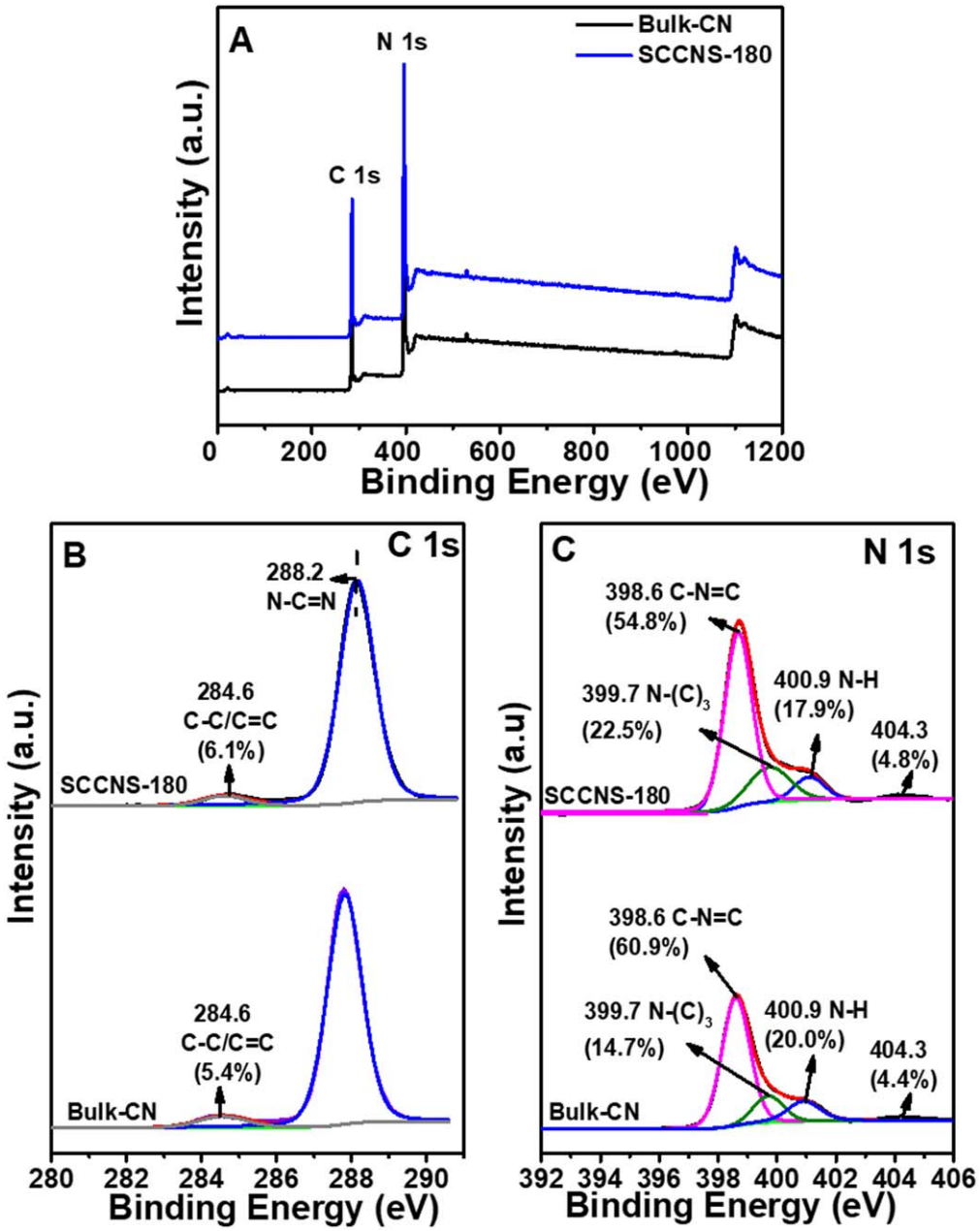

Figure 3. XPS spectra (A), high-resolution C 1s (B) and N 1s (C) spectra of bulk-CN and SCCNS-180.

with bulk-CN, increased from 14.7% to 22.5%, but decreased from 20% to 17.9% at 400.9 eV, suggesting that the carbon-bridged structure in SCCNS-180 was formed because the doping carbon atoms take the place of hydrogen atoms in some of the amino groups (N–H) [57]. Elemental analysis by XPS was also conducted to determine the molar ratio of C/N for bulk-CN and SCCNS-180 (see table S4). Consequently, the C/N ratio was 0.708 and 0.713, respectively, for bulk-CN and SCCNS-180, indicating the characteristic carbon self-doping.

The optical properties of bulk-CN and various SCCNS-T samples are displayed in figure 4. All SCCNS-T samples exhibit much greater visible light absorption ($\lambda > 450$ nm) than bulk-CN (figure 4(A)). Moreover, the band gaps of all samples were calculated by the corresponding Tauc plots (figure 4(B)). It was found that the band gaps of various SCCNS-T samples (2.36, 2.46, 2.37 eV for SCCNS-160, SCCNS-180, SCCNS-200) were slightly more broadened than that of bulk-CN (2.32 eV). Significantly, the additional absorption region of SCCNS-T from 450 to 800 nm derives from the n–π^* electronic transitions involving nitrogen lone pairs, which is allowed for distorted polymeric units but forbidden for planar symmetric *s*-triazine or heptazine structures [58]. Generally, high-temperature calcination in an inert gas atmosphere can improve g-C_3N_4 condensation, whereas we successfully prepared distorted SCCNS-T nanosheets by simple carbon self-doping. The unique distorted SCCNS-T nanosheet structure could cause the intrinsic electron and band structure changes in SCCNS-T [57]. Consistent with the absorption results, bulk-CN and various SCCNS-T samples exhibited a corresponding change in color

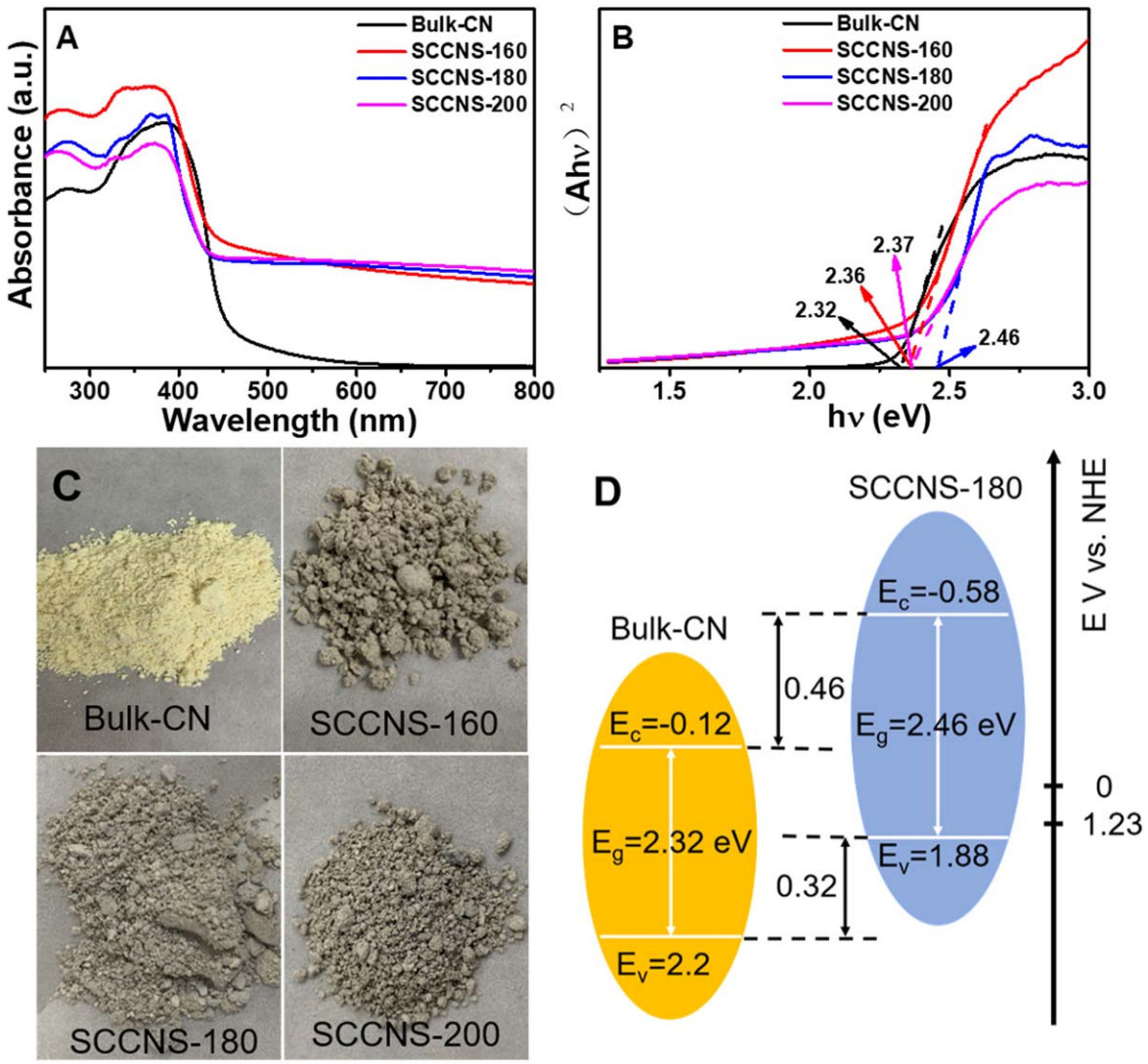

Figure 4. UV–vis diffuse reflectance spectra (A), the corresponding Tauc plots (B) and photographs (C) of bulk-CN and various SCCNS-T samples. (D) Schematic band structures of bulk-CN and SCCNS-180.

from light yellow to gray (figure 4(C)). The band edges of bulk-CN and SCCNS-180 were further studied using valence band (VB) XPS spectra, as shown in figure S3, and the VBs for both were 2.20 and 1.88 eV, respectively. Combined with their band gaps (2.32 and 2.46 eV), the conduction bands (CBs) of bulk-CN and SCCNS-180 were calculated to be −0.12 and −0.58 eV, respectively. Obviously, the CB of SCCNS-180 negatively shifts by 0.46 eV compared with bulk-CN, leading to its enhanced photocatalytic reduction ability for H_2 production. The specific energy band structures of bulk-CN and SCCNS-180 are shown in figure 4(D). Thus, SCCNS-180 with its enlarged specific surface area and enhanced reduction ability could be a superior visible-light responsive photocatalyst for H_2 production.

Since photogenerated charge carrier transfer and separation efficiency greatly affect the photocatalytic performance of photocatalysts, photocurrent density, electrochemical impedance spectroscopy (EIS), photoluminescence (PL) spectroscopy and time-resolved fluorescence decay spectroscopy were conducted for all samples [36]. As shown in figure 5(A), all SCCNS-T samples displayed much enhanced photocurrent density compared with bulk-CN when irradiated with visible light, and the photocurrent densities were about 0.26, 0.60, 0.84 and 1.20 μA cm^{-2} for bulk-CN, SCCNS-200, SCCNS-160 and SCCNS-180, respectively. These trends are consistent with the samples' photocatalytic H_2 evolution performance. The highest photocurrent in SCCNS-180 indicates its superior photogenerated charge carrier separation and transfer rate, which favor its photocatalytic activity. The improved charge carrier transport in SCCNS-T samples can be further verified by the reduced hemicycle radius obtained using EIS, since arc radius is negatively correlated with the charge carrier transfer rate. As shown in figure 5(B), the order of hemicycle radius is bulk-CN > SCCNS-200 > SCCNS-160 > SCCNS-180, suggesting that SCCNS-180 possesses superior charge carrier transfer and greater separation rate; this result is consistent with the photocurrent–time curve. The PL spectrum was also obtained to further characterize the photogenerated charge carrier separation efficiency of bulk-CN and SCCNS-T since PL intensity always reveals the photoinduced electron–hole pair recombination rate. Specifically, a lower PL intensity indicates a decreased photoinduced

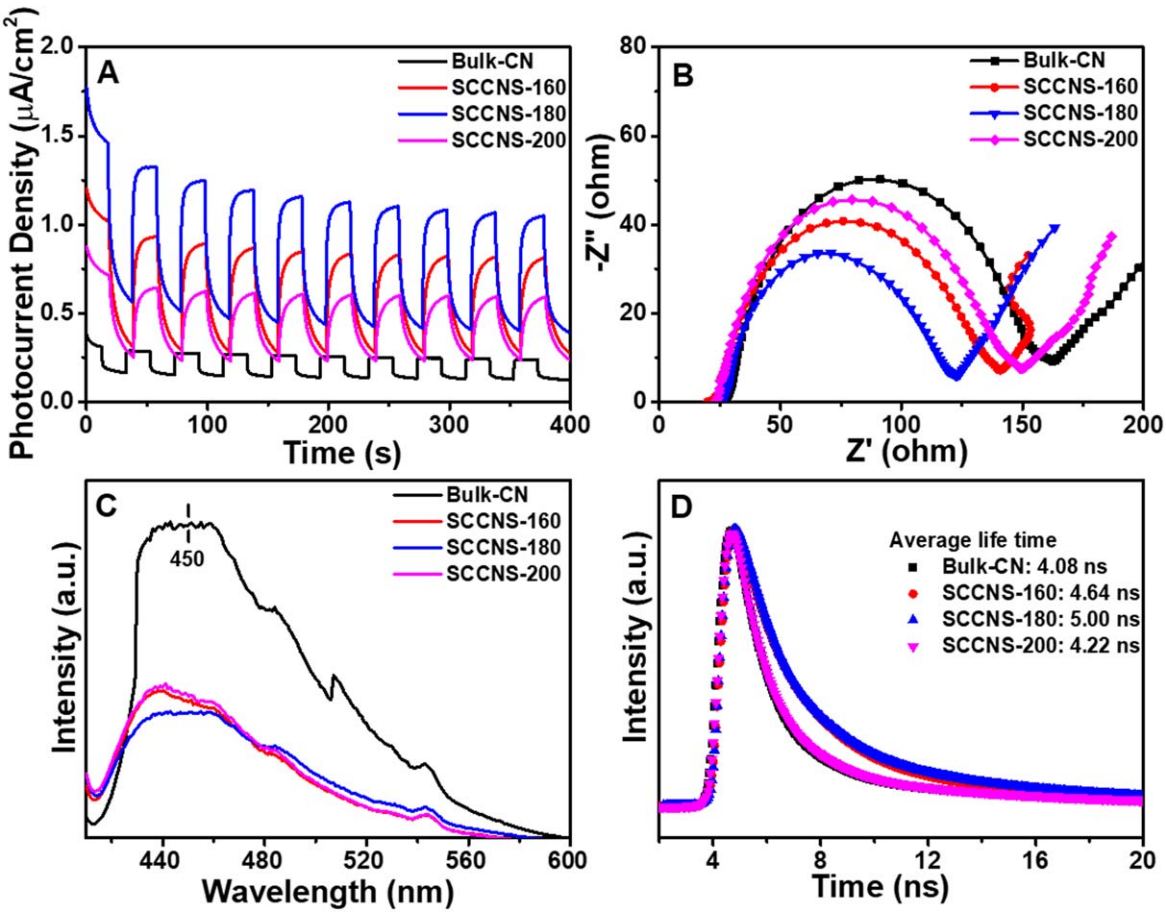

Figure 5. Photocurrent responses (A), EIS Nyquist plots (B), PL emission spectra (λ_{ex} = 400 nm) (C) and time-resolved PL spectra (D) of bulk-CN and various SCCNS-T samples.

electron–hole pair recombination rate [59]. As displayed in figure 5(C), all samples showed a remarkable PL peak at ~450 nm, which represents the direct recombination of photo-induced electron–hole pairs of the band gap. Significantly, the PL emission peaks of all SCCNS-T samples blue-shift slightly, demonstrating their slightly enlarged band gaps. Moreover, the PL intensity of all SCCNS-T samples decreased dramatically compared with bulk-CN, especially for SCCNS-180, indicating a much decreased photoinduced electron–hole pair recombination rate in SCCNS-180. This may be attributed to the unique sponge-like nanosheet structure of SCCNS-180 with self-doped carbon, leading to its shorter charge carrier migration path and improved electronic conductivity, thus suppressing photoinduced electron–hole pair recombination. To further study the photogenerated charge carrier lifetime of samples, time-resolved PL was also performed, and the corresponding fitted parameters can be found in table S5. As shown in figure 5(D), the fluorescent lifetime of SCCNS-180 (τ = 5.00 ns) was prolonged compared with SCCNS-160 (τ = 4.64 ns), SCCNS-200 (τ = 4.22 ns) and bulk-CN (τ = 4.08 ns), indicating its superior charge carrier transfer and separation rate [60, 61].

The photocatalytic H_2 evolution of bulk-CN and SCCNS-T irradiated by visible light ($\lambda > 400$ nm) was evaluated. Both bulk-CN and various SCCNS-T samples exhibit linear increased photocatalytic H_2 production rates (figure 6(A)), demonstrating their excellent photostability. SCCNS-180 exhibits the best photocatalytic H_2 production. The average photocatalytic H_2 production rates of bulk-CN and various SCCNS-T samples are displayed in figure 6(B). All SCCNS-T samples exhibit a higher H_2 evolution rate than bulk-CN, especially SCCNS-180 (~4393 μmol g^{-1} h^{-1}), which is ~17 times as much as bulk-CN (~258 μmol h^{-1} g^{-1}). Moreover, to confirm the stability of SCCNS-180, the H_2 evolution time course of SCCNS-180 is shown in figure 6(C). The yield of H_2 over 4 h continuous irradiation remains almost linear, and hydrogen evolution rate shows no obvious decline within 10 cycles, indicating the superior photocatalytic stability of as-prepared SCCNS-180. Furthermore, the structure and morphology of the fresh and reused SCCNS-180 were also studied by XRD and FETEM (figure S4); the recycled SCCNS-180 sample showed no obvious change, confirming the excellent stability of the as-prepared catalysts. In addition, the QE of SCCNS-180 under illumination by 420 nm monochromatic light was also tested (figure 6(D)). The QE of SCCNS-180 for a wavelength of 420 nm is 6.0%; several reported g-C_3N_4 materials with high QE and H_2 evolution rate are summarized in table S6. SCCNS-180 shows much better catalytic performance, indicating its relatively good utilization of visible light . Furthermore, the photocatalytic H_2 production activity of bulk-CN and various SCCNS-T samples under irradiation with a 300 W Xe lamp were also

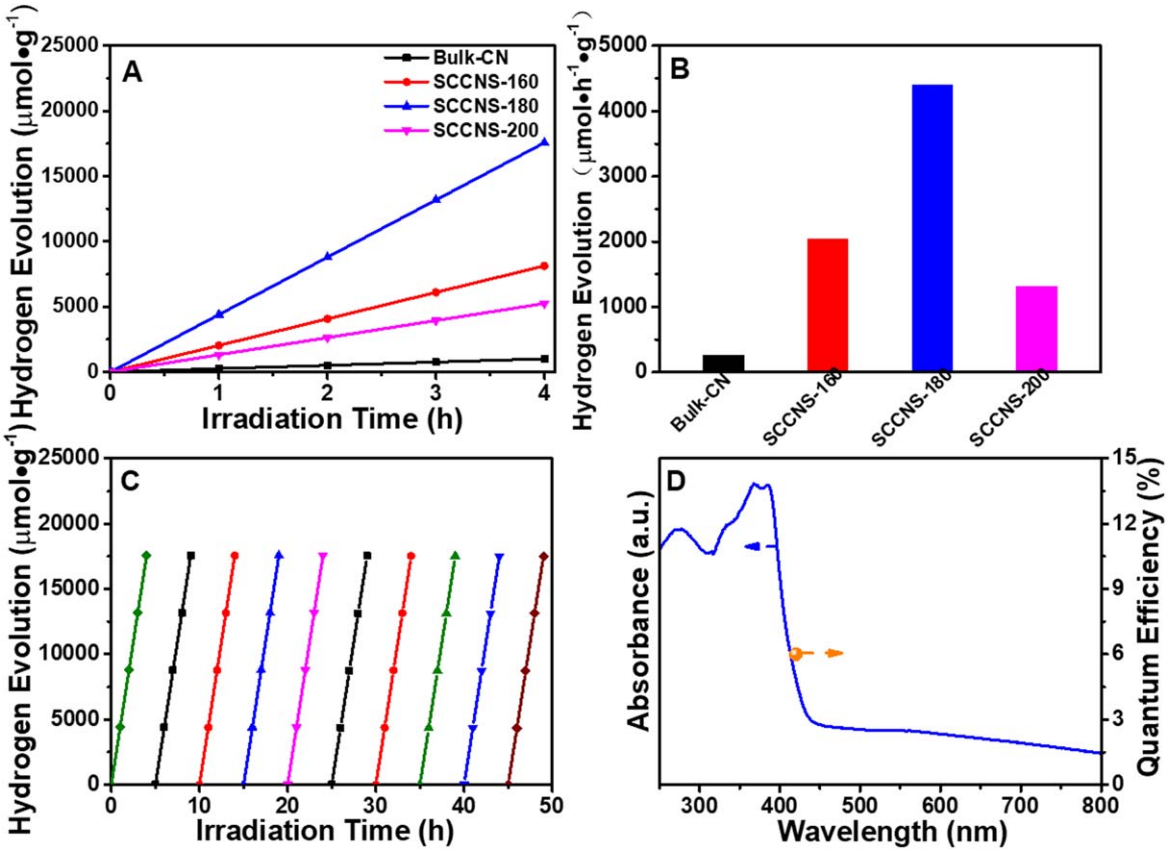

Figure 6. Photocatalytic H_2 production over time (A) and average photocatalytic H_2 evolution rates for bulk-CN and various SCCNS-T samples. The stability of photocatalytic H_2 evolution (C) and QE with a 420 nm band-pass filter (D) for SCCNS-180.

tested (see figure S5); SCCNS-180 also exhibited the most remarkable photocatalytic H_2 evolution activity (~11 320 μmol h^{-1} g^{-1}), ~18 times higher than that of bulk-CN (~620 μmol h^{-1} g^{-1}), indicating its excellent photocatalytic activity under solar light. The photocatalytic H_2 evolution performance of SCCNS-180 in aqueous solution with different sacrificial agents was also investigated and the results are shown in figure S6. It was found that compared with the optimum sacrificial agent (triethanolamine) used in the present work, another commonly used sacrificial agent, namely methanol, showed much lower H_2 evolution activity; work on the intrinsic correlation of the structure of SCCNS-180 with the type of sacrificial agent is under way and will be reported later.

Considering the high performance of g-C_3N_4 cocatalysts in improving photocatalytic H_2 evolution and the limitation of the noble metal Pt because of its low abundance and high price [32–34], our aim is to improve the photocatalytic H_2 evolution performance of as-prepared SCCNS-180 by compositing it with efficient non-noble metal and/or metal-free cocatalysts, including graphene, black phosphorus, NiS, CoP and MoS_X; work on this is currently under way.

4. Conclusions

In summary, we have developed novel sponge-like carbon self-doping g-C_3N_4 nanosheets with a well-organized, highly crystalline, large specific surface area structure and excellent conductivity. Synthesis is via simple one-step calcination of a supramolecular precursor obtained from a combination of the supramolecular pre-assembly (including melamine, cyanuric acid and EG) and the solvothermal pre-treatment. The as-prepared SCCNS-180 exhibits the following advantages: (a) enhanced visible absorption; (b) reduced charge carrier combination rate; (c) enlarged surface area and thus many more reactive sites; and (d) improved photoreduction activity. As a result, SCCNS-180 exhibited a dramatic visible light ($\lambda > 400$ nm) and simulated sunlight-driven photocatalytic H_2 evolution performance, with the H_2 evolution rate reaching ~4393 and ~11 320 μmol h^{-1} g^{-1}, respectively, which is ~17 and ~18 times as much as bulk-CN (~258 and 620 μmol h^{-1} g^{-1}). Moreover, the QE of SCCNS-180 over 420 nm can reach 6.0%. The present work introduces a feasible means to prepare a well-organized, highly crystalline and carbon self-doping g-C_3N_4 photocatalyst for superior photocatalytic H_2 production.

Acknowledgments

This work was financially supported by the Natural Science Foundation of Shanghai (19ZR1403500), the National Natural Science Foundation of China (NNSFC, Project 21373054) and the Natural Science Foundation of Shanghai Science and Technology Committee (19DZ2270100).

Conflicts of interest

The authors declare no competing financial interest.

ORCID iDs

Wei-Lin Dai https://orcid.org/0000-0003-4838-5678

References

[1] Child M, Koskinen O, Linnanen L and Breyer C 2018 *Renew. Sust. Energ. Rev.* **91** 321
[2] Wang Y-J, Long W, Wang L, Yuan R, Ignaszak A, Fang B and Wilkinson D P 2018 *Energ. Environ. Sci.* **11** 258
[3] Wei Z, Liu M, Zhang Z, Yao W, Tan H and Zhu Y 2018 *Energ. Environ. Sci.* **11** 2581
[4] Liao G, Gong Y, Zhang L, Gao H, Yang G-J and Fang B 2019 *Energ. Environ. Sci.* **12** 2080
[5] Wang Y, Suzuki H, Xie J, Tomita O, Martin D J, Higashi M, Kong D, Abe R and Tang J 2018 *Chem. Rev.* **118** 5201
[6] Reilly K, Fang B, Taghipour F and Wilkinson D P 2017 *J. Catal.* **353** 63
[7] Wang Y-J, Chang G, Chen Q, Yang G-J, Fan S-Q and Fang B 2015 *Chem. Commun.* **51** 685
[8] Yang S-C, Chang G, Yang G-J, Wang Y-J and Fang B 2015 *Catal. Sci. Technol.* **5** 228
[9] Ran J, Ma T Y, Gao G, Du X-W and Qiao S Z 2015 *Energ. Environ. Sci.* **8** 3708
[10] Ni M, Leung M K H, Leung D Y C and Sumathy K 2007 *Renew. Sust. Energ. Rev.* **11** 401
[11] Li P, Chen X, He H, Zhou X, Zhou Y and Zou Z 2018 *Adv. Mater.* **30** 1703119
[12] Ma D, Wu J, Gao M, Xin Y, Ma T and Sun Y 2016 *Chem. Eng. J.* **290** 136
[13] Cui C, Li S, Qiu Y, Hu H, Li X, Li C, Gao J and Tang W 2017 *Appl. Catal.* B **200** 666
[14] Yuan Y-J, Chen D, Yang S, Yang L-X, Wang J-J, Cao D, Tu W, Yu Z-T and Zou Z-G 2017 *J. Mater. Chem.* A **5** 21205
[15] Wang J *et al* 2017 *ACS Appl. Mater. Inter.* **9** 381
[16] Cao S and Yu J 2014 *J. Phys. Chem. Lett.* **5** 2101
[17] Wang X, Maeda K, Thomas A, Takanabe K, Xin G, Carlsson J M, Domen K and Antonietti M 2009 *Nat. Mater.* **8** 76
[18] Wang Y, Wang X and Antonietti M 2012 *Angew. Chem. Int. Edit.* **51** 68
[19] Liu J, Zhang T, Wang Z, Dawson G and Chen W 2011 *J. Mater. Chem.* **21** 14398
[20] Zhu B, Xia P, Ho W and Yu J 2015 *Appl. Surf. Sci.* **344** 188
[21] Chung H T, Johnston C M, Artyushkova K, Ferrandon M, Myers D J and Zelenay P 2010 *Electrochem. Commun.* **12** 1792
[22] Groenewolt M and Antonietti M 2005 *Adv. Mater.* **17** 1789
[23] Liang Q, Huang Z-H, Kang F and Yang Q-H 2015 *ChemCatChem* **7** 2897
[24] Cui Y, Zhang J, Zhang G, Huang J, Liu P, Antonietti M and Wang X 2011 *J. Mater. Chem.* **21** 13032
[25] Fang S, Xia Y, Lv K, Li Q, Sun J and Li M 2016 *Appl. Catal.* B **185** 225
[26] Cheng F, Wang H and Dong X 2015 *Chem. Commun.* **51** 7176
[27] Zhou Z, Zhang Y, Shen Y, Liu S and Zhang Y 2018 *Chem. Soc. Rev.* **47** 2298
[28] Lv Y, Chen S, Shen Y, Ji J, Zhou Q, Liu S and Zhang Y 2018 *J. Am. Chem. Soc.* **140** 2801
[29] Chen S, Lv Y, Shen Y, Ji J, Zhou Q, Liu S and Zhang Y 2018 *ACS Appl. Mater. Inter.* **10** 6887
[30] Lin Z and Wang X 2013 *Angew. Chem. Int. Edit.* **52** 1735
[31] Lin L, Ou H, Zhang Y and Wang X 2016 *ACS Catal.* **6** 3921
[32] Shen R, Liu W, Ren D, Xie J and Li X 2019 *Appl. Surf. Sci.* **466** 393
[33] Lu X, Xie J, Liu S-Y, Adamski A, Chen X and Li X 2018 *ACS Sustain. Chem. Eng.* **6** 13140
[34] Wen J, Xie J, Shen R, Li X, Luo X, Zhang H, Zhang A and Bi G 2017 *Dalton Trans.* **46** 1794
[35] Liang Z, Shen R, Ng Y H, Zhang P, Xiang Q and Li X 2020 *J. Mater. Sci. Technol.* **56** 89
[36] Shen R, Xie J, Xiang Q, Chen X, Jiang J and Li X 2019 *Chinese J. Catal.* **40** 240
[37] Li Y, Jin Z, Zhang L and Fan K 2019 *Chinese J. Catal.* **40** 390
[38] Li Z, Ma Y, Hu X, Liu E and Fan J 2019 *Chinese J. Catal.* **40** 434
[39] Ren D, Zhang W, Ding Y, Shen R, Jiang Z, Lu X and Li X 2020 *Solar RRL* **4** 1900423
[40] Wang X, Maeda K, Chen X, Takanabe K, Domen K, Hou Y, Fu X and Antonietti M 2009 *J. Am. Chem. Soc.* **131** 1680
[41] Han Q, Wang B, Gao J, Cheng Z, Zhao Y, Zhang Z and Qu L 2016 *ACS Nano* **10** 2745
[42] Xiong T, Cen W, Zhang Y and Dong F 2016 *ACS Catal.* **6** 2462
[43] Liu Q, Wang X, Yang Q, Zhang Z and Fang X 2018 *Appl. Catal.* B **225** 22
[44] Hong Y, Li C, Fang Z, Luo B and Shi W 2017 *Carbon* **121** 463
[45] Dong G, Zhao K and Zhang L 2012 *Chem. Commun.* **48** 6178
[46] Gao H, Cao R, Zhang S, Yang H and Xu X 2019 *ACS Appl. Mater. Inter.* **11** 2050
[47] Yu H, Shi R, Zhao Y, Bian T, Zhao Y, Zhou C, Waterhouse G I N, Wu L-Z, Tung C-H and Zhang T 2017 *Adv. Mater.* **29** 1605148
[48] Fang Z, Hong Y, Li D, Luo B, Mao B and Shi W 2018 *ACS Appl. Mater. Inter.* **10** 20521
[49] Han Q, Wang B, Zhao Y, Hu C and Qu L 2015 *Angew. Chem. Int. Edit.* **54** 11433
[50] She X, Xu H, Xu Y, Yan J, Xia J, Xu L, Song Y, Jiang Y, Zhang Q and Li H 2014 *J. Mater. Chem.* A **2** 2563
[51] Li X, Pan K, Qu Y and Wang G 2018 *Nano Res.* **11** 1322
[52] Huang Y, Li D, Fang Z, Chen R, Luo B and Shi W 2019 *Appl. Catal.* B **254** 128
[53] She X, Xu H, Wang H, Xia J, Song Y, Yan J, Xu Y, Zhang Q, Du D and Li H 2015 *Dalton Trans.* **44** 7021
[54] Zhang J, Zhang M, Yang C and Wang X 2014 *Adv. Mater.* **26** 4121
[55] Mo Z *et al* 2018 *Appl. Catal.* B **225** 154
[56] Liang Q, Li Z, Huang Z-H, Kang F and Yang Q-H 2015 *Adv. Funct. Mater.* **25** 6885
[57] Su F-Y, Xu C-Q, Yu Y-X and Zhang W-D 2016 *ChemCatChem* **8** 3527
[58] Jorge A B *et al* 2013 *J. Phys. Chem.* C **117** 7178
[59] Fang J, Fan H, Zhu Z, Kong L B and Ma L 2016 *J. Catal.* **339** 93
[60] Li Y, Yang M, Xing Y, Liu X, Yang Y, Wang X and Song S 2017 *Small* **13** 1701552
[61] Chen Z, Fan T-T, Yu X, Wu Q-L, Zhu Q-H, Zhang L-Z, Li J-H, Fang W-P and Yi X-D 2018 *J. Mater. Chem.* A **6** 15310